

Nanoconfined catalytic Ångström-size motors

Peter H. Colberg^{1, a)} and Raymond Kapral^{1, b)}

Chemical Physics Theory Group, Department of Chemistry, University of Toronto, Toronto, Ontario M5S 3H6, Canada

Self-propelled chemically powered synthetic micron and nano-scale motors are being intensively studied because of the wide range of potential applications that exploit their directed motion. This paper considers even smaller Ångström-size synthetic motors. Such very small motors in bulk solution display effects arising from their self-propulsion. Recent experiments have shown that small-molecule catalysts and single enzyme molecules exhibit properties that have been attributed to their chemical activity. Molecular dynamics is used to investigate the properties of very small Ångström-size synthetic chemically powered sphere-dimer motors in a simple atomic-like solvent confined between walls separated by distances of tens of nanometers. Evidence for strong structural ordering of the motors between the walls, which reflects the finite size of solvent molecules and depends on solvent depletion forces, is provided. Dynamical properties, such as average motor velocity, orientational relaxation, and mean square displacement, are anisotropic and depend on the distance from the walls. This research provides information needed for potential applications that use molecular-scale motors in the complex confined geometries encountered in biology and the laboratory.

I. INTRODUCTION

Synthetic self-propelled motors that convert chemical energy from their environment into directed motion are examples of active objects with distinctive and useful properties. Much of the interest in such motors stems from potential applications that exploit their directed motion to carry out functions involving cargo transport, analogous to the active transport tasks performed by molecular motors in the cell.^{1–5}

In many circumstances, motors operate in complex environments or systems confined by boundaries. Examples include motors used in microfluidic devices⁶ and potential *in vivo* applications such as targeted drug delivery^{7,8}. Also, in many experiments currently being carried out, motors reside near a surface as a result of gravitational or other forces, and the interactions of motors with surfaces can lead to interesting dynamical effects.^{9–12} For these reasons, it is important to assess the influence of boundaries and confinement on motor dynamics.

The effects of confinement on motor motion have been investigated previously. The velocity of a spherical self-propelled particle with a point-like catalytic site confined by a spherical wall has been computed analytically.¹³ Micron-scale Janus motors operating by self-diffusiophoresis have been studied experimentally and numerically in circumstances where they collide with a wall, are confined to a circular pore, and move through a triangular lattice of obstacles forming a patterned environment.¹⁴ The dynamics of a self-diffusiophoretic Janus particle close to a hard wall has been shown to exhibit reflection, steady sliding, and hovering.¹⁵ A study of such Janus particles near a wall has been carried out using continuum hydrodynamics.¹⁶ The rectification of a Brownian Janus particle in a triangular channel¹⁷

and the escape of an ellipsoidal Brownian Janus particle from a two-dimensional sinusoidally corrugated or square-shaped pore have been simulated.¹⁸ Studies of confined self-propelled rods have shown that they tend to reside near surfaces.¹⁹ The accumulation of self-propelled Brownian spheres near a hard wall has been studied analytically and simulated using multi-particle collision dynamics.²⁰ Similarly, ensembles of self-propelled colloidal rods aggregate and structurally order on confining walls.²¹

In a related but somewhat different context, the effects of hydrodynamic interactions on the confined motions of swimmers and biological organisms have also been investigated. Since biological organisms function in environments containing obstacles and boundaries of various types, such studies are essential in order to obtain a full understanding of swimming motions in a biological context. Studies of hydrodynamic effects on self-propulsion of both synthetic swimmers and biological organisms near boundaries and in complex media have been carried out.^{21–26} Boundaries can influence the collective behavior of swimmers and the collective motions of swimmers confined to the gap between two planar surfaces have been observed.^{24,25}

Several factors must be considered in order to understand the effects of confinement on chemically powered motors. These include direct interactions with the boundaries, motor geometry, the influence of boundaries on hydrodynamic flows, and the nature of chemical gradients near walls. At the micron to nanometer scales, self-propulsion is influenced by thermal fluctuations. Orientational Brownian motion limits the duration of the ballistic regime where directed motion can be observed and leads to diffusive dynamics on long time scales, albeit characterized by diffusion coefficients that reflect the underlying active motion. Interactions with boundaries can influence orientational Brownian motion and modify motor behavior.

In this paper, we consider a regime of motor dynamics and confinement that differs from that in earlier inves-

^{a)} Electronic mail: pcolberg@chem.utoronto.ca

^{b)} Electronic mail: rkapral@chem.utoronto.ca

tigations. We focus on very small Ångström-scale motors confined in thin nanometer-scale layers between two walls. This study is prompted by several observations. Recent experiments have demonstrated that catalytically active 5 Å organometallic molecules²⁷ as well as single enzyme molecules^{28,29} display enhanced diffusion compared to the same systems in the absence of chemical activity. In addition, experimental studies of very small (30 nm) synthetic self-propelled Janus particles have also found enhanced diffusion coefficients.³⁰ Although the precise mechanism responsible for diffusion enhancement is still a matter of debate for the molecular systems, the observed phenomena are correlated with chemical activity. Such enzymatically induced motion has been reviewed recently.³¹ In addition to these experimental results, molecular dynamics simulations of chemically propelled Ångström-size sphere-dimer motors that operate by self-diffusiophoresis have shown that these motors can move distances of one to several times their length before they reorient and have enhanced diffusion coefficients.³²

For such small-scale motors, whose size is comparable to the molecules comprising the environment, solvent structural effects play an important role and fluctuations dominate their behavior. Nevertheless, the signatures of self-propulsion are clearly evident in observable properties such as diffusion coefficients. Enzymes carry out their functions in the complex cellular environment and, potentially, very small synthetic motors will find applications on the cellular level and other confined systems. It is then important to consider effects due to the confinement on these very small motors.

System-specific features of both the motor and solvent molecules can determine the structural and dynamical properties of motors with small molecular-scale dimensions. Some general properties are common to all such motors. Small motors reorient very rapidly, for example, nanometer-scale motors have reorientation times of the order of nanoseconds or picoseconds, compared to times of the order of seconds for micron-sized motors. This time scale disparity will have an effect on the relative importance of ballistic and diffusive motions. For small motors, solvent structural correlations can influence effective motor-wall forces in confined systems, as well as the concentrations of fuel species in the motor vicinity. Although the quantitative form these effects take depends on the system under study, their presence is a common feature of molecular-scale motors. In this study, we consider a simple dimer motor made from catalytic and noncatalytic spheres in a dense atomic-like solvent in order to investigate some of the general aspects of solvent and confinement effects on very small motors.

The outline of the paper is as follows: In Sec. II, we describe the model for the motor and solvent molecules, along with their interactions with the confining walls. Section III presents results on static structural properties, in particular, the nature of the motor position and its angular distributions perpendicular and parallel to the walls. Dynamical properties, including dimer velocity,

orientational correlations, and mean square displacement (MSD), are discussed in Sec. IV. The conclusions of the study are given in Sec. V.

II. CONFINED SELF-PROPELLED MOTORS

We consider motors that achieve propulsion by utilizing catalytic reactions through a self-diffusiophoretic mechanism.^{5,33–35} In this mechanism, a chemical reaction on a portion of the motor leads to asymmetric distributions of reactants and products in the motor vicinity. If the reactants and products interact with the motor through different intermolecular potentials, this gives rise to a body force on the motor. Since no external forces are applied to the system, the entire system, the motor and its environment, are force-free, and momentum conservation leads to fluid flows in the environment. This mechanism is responsible for the directed self-propelled motion of such motors.

The most widely studied motors of this type are Janus colloids where one face is catalytic and the other chemically neutral. Suppose that the chemical reaction $A \rightarrow B$ occurs on the catalytic face and the A and B molecules interact with the Janus particle through $U_{J,A}$ and $U_{J,B}$ intermolecular potentials. Using the equations of continuum hydrodynamics, supplemented with boundary conditions that account for reactions and fluid velocities on the surface of the Janus particle, the velocity of the motor is given by

$$V = (k_B T / \eta) \Lambda_J \langle \hat{z} \cdot \nabla_\theta c_B(r_J, \theta) \rangle_S, \quad (1)$$

where \hat{z} is a unit vector from the noncatalytic to catalytic faces of the Janus particle, $c_B(r_J, \theta)$ is the concentration of species B on the surface as a function of the angle θ , $\langle \dots \rangle_S$ denotes the average over the spherical surface, and

$$\Lambda_J = \int_0^\infty dr r [e^{-\beta U_{J,B}(r)} - e^{-\beta U_{J,A}(r)}], \quad (2)$$

with $\beta = 1/(k_B T)$. From this expression, we see that the velocity depends on the surface average of the gradient of the concentration along the surface, the difference in the interaction potentials as determined by Λ_J and η , the viscosity of the solution. These are features of all motors that operate by diffusiophoretic mechanisms.

Motor geometry is a factor to consider when dealing with wall interactions, and instead of spherical Janus motors, we investigate the dynamics of sphere-dimer motors that are simple examples of more complex, non-spherical motors. A sphere-dimer consists of linked catalytic (C) and noncatalytic (N) spheres. In this geometry, the catalytic region is restricted to one sphere.³⁶ The directed motion of the motor is again due to a diffusiophoretic mechanism. Experimental¹¹ and simulation^{37–39} studies of the motions of sphere-dimer motors in bulk solution have been performed. The analytic continuum theory for the velocity of a sphere-dimer motor is considerably

more involved due to the motor geometry, but it may be obtained using a bispherical coordinate system.^{40,41} The theory predicts that the velocity of the motor along the dimer bond is given by a form analogous to that for the Janus particle,

$$V = (k_B T / \eta) \Lambda_{SD} K, \quad (3)$$

with K given by a complicated but explicit expression⁴¹ that plays the same role as the surface average of the concentration gradient for the Janus particle. If the intermolecular potentials only differ for interactions of A and B with the noncatalytic sphere, Λ_{SD} has the form

$$\Lambda_{SD} = \int_0^\infty dr \, r [e^{-\beta U_{N,B}(r)} - e^{-\beta U_{N,A}(r)}]. \quad (4)$$

Since we are interested in very small Ångström-scale motors, continuum theory is not able to describe all relevant effects. As noted earlier, fluctuations are especially important and the finite size of the solvent molecules is comparable to that of the motor, both of which violate the assumptions of a continuum description of the solvent. Instead we adopt a full molecular dynamics description of a self-propelled Ångström-scale motor confined between two parallel walls.

In more detail, the sphere-dimer motor we consider consists of a catalytic C sphere and a noncatalytic N sphere, with diameters $\sigma_C = 2\sigma$ and $\sigma_N = 4\sigma$, respectively, linked by a rigid bond of length d . While various dimer-sphere sizes can be chosen, and the results will depend on these values, we have selected a sphere-diameter ratio of $\sigma_C/\sigma_N = 0.5$ that has been shown to yield the highest propulsion velocity both experimentally¹¹ and theoretically⁴¹. The solvent consists of N_s structureless A and B particles with diameter σ and mass m . The solvent number density is $\rho_s = N_s/V = 0.8\sigma^{-3}$, which corresponds to a dense fluid. The sphere dimer masses, $M_m = \frac{\pi}{6}\rho_s m(\sigma_C^3 + \sigma_N^3)$, are chosen to make the dimer neutrally buoyant. All particles interact through a shifted, truncated Lennard-Jones potential, $V_{ij}(r) = \epsilon_{ij} \{4[(\sigma_{ij}/r)^{12} - (\sigma_{ij}/r)^6] + 1\}$ for $r < \sqrt[3]{2}\sigma_{ij}$ and zero otherwise. Here r is the distance between the centres of a pair of particles, $\sigma_{CA} = \sigma_{CB} = \frac{1}{2}(\sigma_C + \sigma)$ and $\sigma_{NA} = \sigma_{NB} = \frac{1}{2}(\sigma_N + \sigma)$ for pairs of dimer sphere and solvent particle, and $\sigma_{AA} = \sigma_{AB} = \sigma_{BB} = \sigma$ for pairs of solvent particles. The interaction energy is ϵ for all pairs apart from NB pairs, where $\epsilon_{NB} = 0.1\epsilon$ or 10ϵ . The temperature of the system is $k_B T / \epsilon = 1$.

The system is contained in a slab with edge lengths $L_X = L_Y = 50\sigma$ and $L_Z = 10, 15, \dots, 50\sigma$ with periodic boundary conditions in X and Y directions and two planar walls at $Z = 0$ and L_Z . The dimer spheres and solvent particles interact with the walls via a repulsive 9-3 Lennard-Jones potential, $V_S(\zeta) = \epsilon_{wS} \{(3\sqrt{3}/2)[(\sigma_{wS}/\zeta)^9 - (\sigma_{wS}/\zeta)^3] + 1\}$ for $\zeta < \sqrt[3]{3}\sigma_{wS}$, where ζ is the distance to the closest wall, and zero otherwise. The wall interaction parameters are $\sigma_{wA} = \sigma_{wB} =$

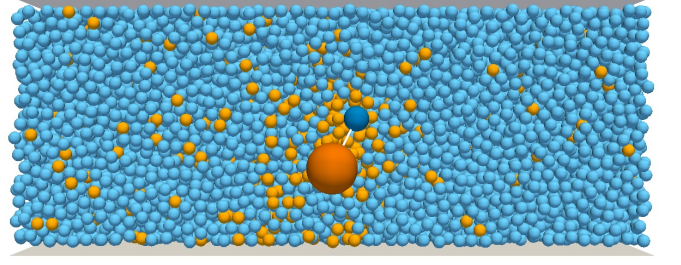


FIG. 1. Cross section of sphere-dimer motor with spheres C (blue) and N (vermilion) immersed in A (sky blue) and B (orange) solvent particles confined between two planar walls a distance $L_Z = 20$ apart.

σ , $\sigma_{wC} = (\sigma_C + \sigma)/2$, $\sigma_{wN} = (\sigma_N + \sigma)/2$, $\epsilon_{wA} = \epsilon_{wB} = \epsilon$, and $\epsilon_{wC} = \epsilon_{wN} = \epsilon$ or 2ϵ .

The C sphere catalyses the reaction $A \rightarrow B$, where A is converted to B with unit probability when it lies within a distance $\sqrt[3]{2}\sigma_{CB}$ from the C sphere. The system is maintained in a nonequilibrium steady state through a bulk back-reaction $B \rightarrow A$ with rate $10^{-3}\tau^{-1}$ outside of the C- and N-sphere interaction zones. The dimer bond length is taken to be $d = \sqrt[3]{2}(\sigma_{CB} + \sigma_{NB})$, which is chosen to ensure energy conservation in the presence of reactions.

Full molecular dynamics⁴² is used to follow the motions of the motor and solvent and capture their structural and dynamical properties.⁴³ The model neglects the structure of the solvent molecules, but nevertheless it is suited to reproduce structural and dynamical effects occurring at the Ångström scale. As discussed in the Introduction, applications to experimental systems should take into account the detailed structural properties of the motor and solvent under investigation. The velocity-Verlet integration time step for the molecular dynamics simulations is $10^{-3}\tau$. Simulation results are reported in dimensionless units with distance given in units of σ , mass in units of m , energy in units of ϵ , and time in units of $\tau = \sigma\sqrt{m\epsilon^{-1}}$.

Parameters were chosen to model a dense fluid Argon-like solvent. Given Argon⁴⁴ values of $\sigma = 0.34$ nm, $\epsilon = 120$ K k_B , and $m = 39.95$ u and $\tau = 2.15$ ps, we can assign physical values to our Ångström-scale motor simulations. In these units the sphere-dimer monomers have radii of 0.34 nm and 0.68 nm for the C and N spheres, respectively. The end-to-end length of the sphere-dimer motor is 2.55 nm. The separation between the walls varies from 3.4 nm to 17 nm.

The continuum theory for sphere-dimer motors that operate by self-diffusiophoresis has been carried out^{40,41} and the fluid flow fields associated with propulsion have been determined⁴¹. Motors with $\epsilon_{NB} = 0.1$ and small dimer bond lengths move in the direction of the C sphere and the far-field fluid flow is characteristic of a puller. For $\epsilon_{NB} = 10$, the motor is propelled in the direction of the N sphere and the far-field fluid flow is characteristic of a pusher. Both types of motor were investigated in

confinement between two planar walls, and in bulk with periodic boundary conditions in all directions.

To isolate effects that are due to the self-propulsion of the motor, results for an inactive dimer ($\epsilon_{NB} = 1$) are also presented. Inactive dimers were constructed by turning off the chemical reactions that power the motor and maintain the system in a nonequilibrium steady state. The effect of the wall potential on the dimer is illustrated by varying the repulsiveness between walls and spheres, denoted in the following as the weaker ($\epsilon_{wS} = 1$) and the stronger wall potential ($\epsilon_{wS} = 2$).

An instantaneous configuration of the sphere dimer and surrounding A and B solvent species confined between two walls is shown in Fig. 1. In this figure one can see the relative sizes of dimer monomers and solvent particles, as well as the inhomogeneous distribution of reactants and products near the dimer and wall, which will play an important role in the subsequent discussion.

III. STRUCTURAL ORDERING OF DIMER MOTOR IN CONFINED GEOMETRY

We consider the structural ordering of the sphere-dimer motor when it is confined between the two walls. Sample trajectories of an inactive dimer, and puller and pusher motors are shown in Fig. 2. The dimer is initially placed along the middle plane between the walls. Depending on the absence or presence of propulsion, the dimer takes a long or short time, respectively, until its first contact with a wall. In the case of the inactive dimer and the pusher motor, once the dimer has reached a wall, it remains close to the wall for the remaining time. The larger N sphere resides at a fixed distance from the wall. This effective attraction to the wall is explained by the strong solvent depletion force⁴⁵ between the wall and the sphere. The smaller C sphere experiences a negligible depletion force, which allows the sphere to freely explore the wall region that lies within the constraints of the dimer bond. The degree of repulsiveness of the wall has no discernible effect on the motion of the inactive dimer or the pusher motor after being trapped by the wall. The puller motor on the other hand behaves very differently depending on the strength of the wall potential. For the weaker wall repulsive potential, the puller motor is attached to the wall most of the time as well. In contrast to the inactive dimer and the pusher motor, however, the puller motor occasionally detaches and makes transitions to the opposite wall or returns to the original wall. For the stronger wall repulsive potential, the puller motor is no longer trapped by the walls and frequently makes transitions between them.

The different behaviors of the pusher versus puller motor are a consequence of the respective direction of propulsion. When the dimer bond is perpendicular to the wall, the propulsion force of the pusher motor acts in the same direction as the depletion force on the N sphere, which reinforces the trapping by the wall. The propul-

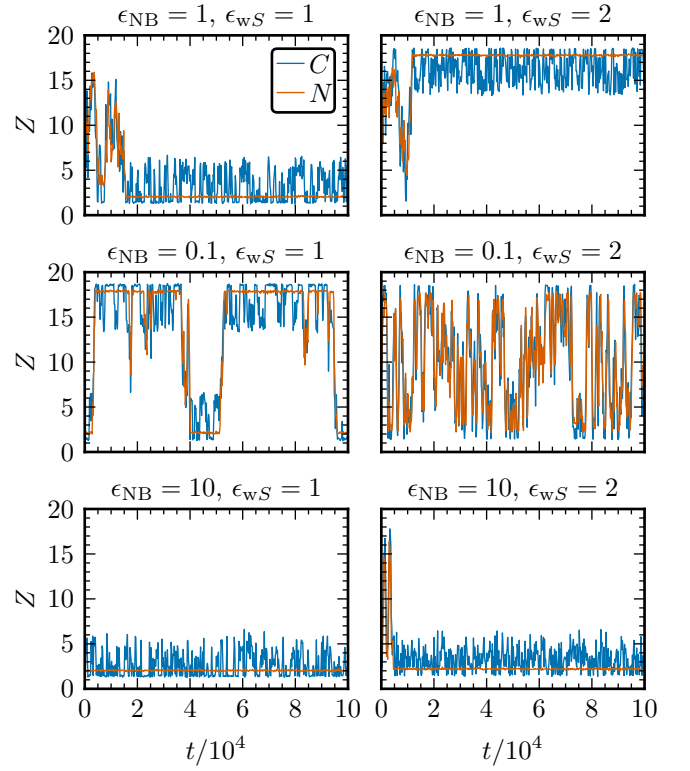


FIG. 2. Trajectories of the perpendicular distances of the N (red) and C (blue) dimer spheres to walls, Z , versus time for an inactive dimer (top), and puller (middle) and pusher motors (bottom). The left and right panels illustrate a weaker and a stronger repulsiveness of the wall-sphere potential, respectively. The separation between the walls is $L_Z = 20$.

sion force of the puller motor opposes the depletion force, which allows the motor to detach from the wall occasionally or frequently depending on the wall repulsiveness.

The time- and ensemble-averaged⁴⁶ probability densities of N and C sphere positions are shown in Fig. 3 for the stronger wall potential for an inactive dimer, and puller and pusher motors. The insets of Fig. 3 show the probability densities plotted as cumulative distributions. The N sphere density for the inactive dimer and the pusher motor exhibits a pronounced peak, which is the signature of the trapping. Since the time until first contact with a wall is shorter for the pusher motor than for the inactive dimer, the peak magnitude of the N sphere density for the pusher motor is slightly larger and accounts for close to 100% of the corresponding cumulative density. The N sphere density for the puller motor shows a richer structure with damped oscillations that originate from the structural ordering of the atomic-like solvent at the wall. The C sphere density has damped oscillations for all three cases. Far from the wall, the C sphere density converges to a uniform density for the puller motor and decays to zero for the inactive dimer and the pusher motor, identified earlier as the confinement by the dimer bond.

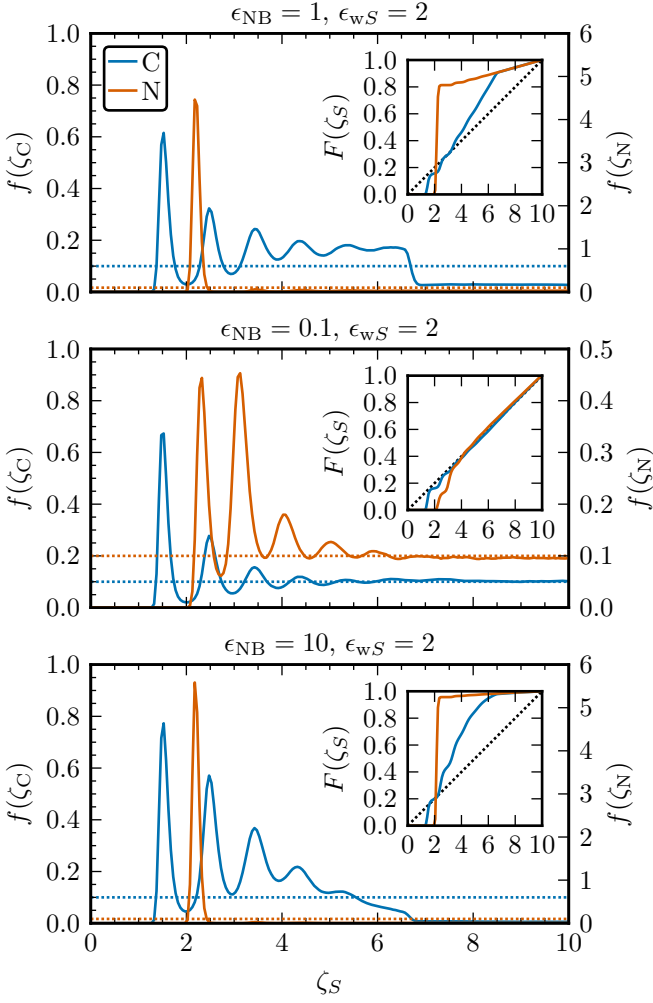


FIG. 3. Probability densities $f(\zeta_S)$ of the distance ζ_S between each dimer sphere S and the nearest wall for an inactive dimer (top), and puller (middle) and pusher motors (bottom), for a wall separation $L_Z = 20$. The insets show the corresponding cumulative probability density $F(\zeta_S)$. The dotted lines indicate uniform density distributions.

The structural ordering of the solvent also affects the average orientation of the dimer relative to the walls. We denote with \mathbf{z} the bond vector pointing along the propulsion direction from the centers of the N to C spheres and separate the contributions perpendicular and parallel to the wall, z_\perp and \mathbf{z}_\parallel , respectively. The probability density of \mathbf{z}_\parallel assumes a uniform distribution due to the periodic boundary conditions in the X and Y directions. The probability density of z_\perp is strongly nonuniform, as seen in Fig. 4, which plots the joint probability density $f(z_\perp, \zeta_N)$ of the perpendicular component of the dimer bond vector, z_\perp , and the distance of the N sphere from the closest wall, ζ_N , for an inactive dimer, and puller and pusher motors. These probability densities were computed by averaging over slabs $[\zeta_N - \frac{\Delta\zeta}{2}, \zeta_N + \frac{\Delta\zeta}{2}]$ of width $\Delta\zeta = 0.4$ parallel to the walls.

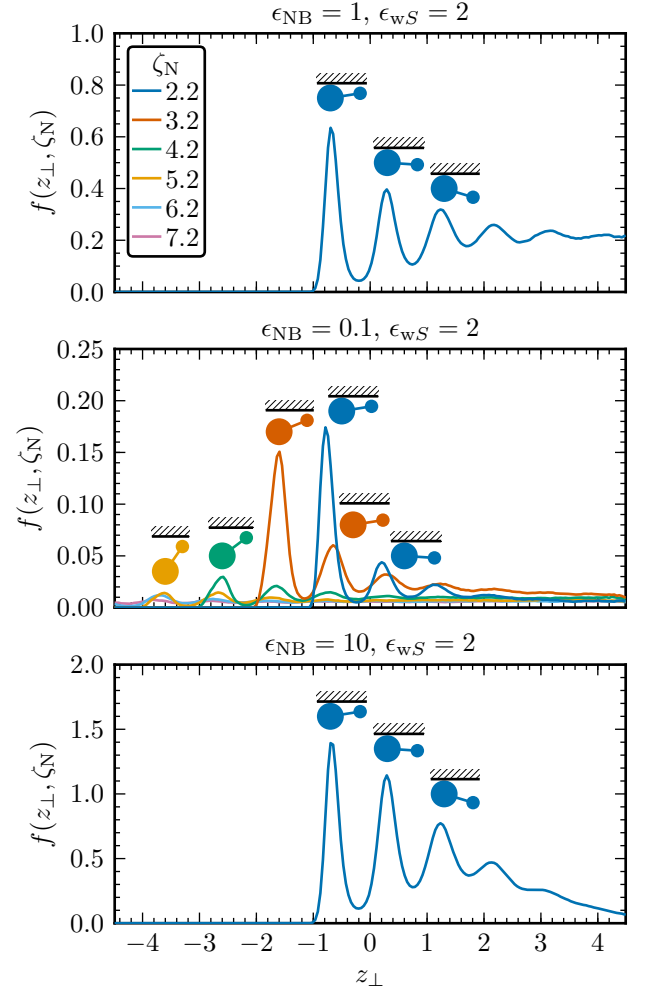


FIG. 4. The joint probability density $f(z_\perp, \zeta_N)$ of the perpendicular component of the dimer bond vector, z_\perp , and the distance of the N sphere from the closest wall, ζ_N , for an inactive dimer (top), and puller (middle) and pusher motors (bottom), for a wall separation $L_Z = 20$. The color coding of the probability densities is indicated in the inset. The dimer configurations associated with the peak maxima are sketched in the figures.

The orientation ranges from $z_\perp = -d$, which corresponds to the dimer being perpendicular to the wall with the C sphere oriented towards the wall, to $z_\perp = d$, which corresponds to the opposite orientation. The densities for all three cases show damped oscillations as a result of solvent structural ordering close to the walls, with a period equal to the diameter of a solvent molecule. Each peak corresponds to a likely configuration of the dimer that is described completely by the dimer bond orientation and the position of the N sphere. The joint probability density $f(z_\perp, \zeta_N)$ plots allow one to assign the motor configurations that contribute most significantly to the peaks of the probability density. These configurations are indicated in the figure.

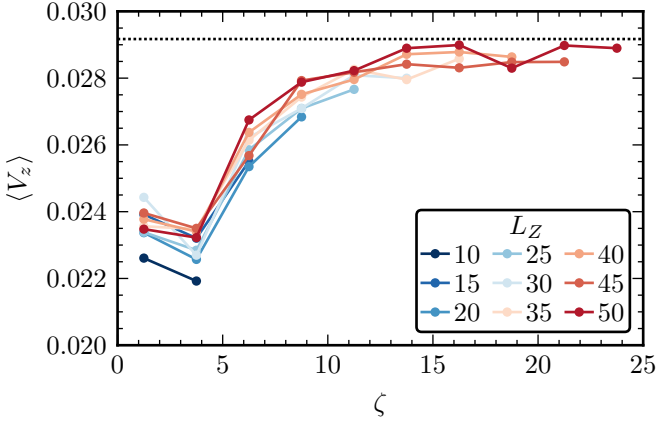


FIG. 5. Mean propulsion velocity, $\langle V_z \rangle$, of a confined puller motor as a function of the distance of its center of mass to the closest wall, ζ , for $\epsilon_{wS} = 2$. The velocities are averaged over slabs $[\zeta - \frac{\Delta\zeta}{2}, \zeta + \frac{\Delta\zeta}{2}]$ of width $\Delta\zeta = 2.5$ parallel to the walls. The dotted line shows the propulsion velocity of an unconfined puller motor.

For the inactive dimer and the pusher motor, the orientation densities resemble the C sphere position densities shown in Fig. 3, which, again, reflects the trapping of the N sphere by the wall. For the inactive dimer, the density converges to a uniform distribution for close-to-perpendicular orientations, while for the pusher motor, the density decays to near zero. This decay follows from the propulsion of the pusher motor parallel to the wall, which causes the C sphere to be pulled along by the trapped N sphere and thereby closer to the wall. Compared to the inactive dimer and the pusher motor, the puller motor exhibits a larger number of likely configurations, since the N sphere is not trapped by the wall.

The effects of confinement on suspensions of hydrodynamically interacting pusher and puller swimmers were investigated by Hernandez-Ortiz et al.²⁵ The swimmers were modeled as dimers comprising beads linked by a stiff spring, subject to a force that gives rise to propulsion. Considering only very low dimer densities, the swimmer concentration profile as a function of the distance from the walls has peaks near the walls. As one moves farther from the walls, the concentration falls to close-to-zero values for pushers and to non-zero values for pullers. These findings are consistent with our puller and pusher single sphere-dimer results. However, we note that our simulations include a variety of other effects including the self-generated chemical gradients, solvent structure and depletion forces, fluctuations as well as hydrodynamics.

IV. MOTOR DYNAMICS IN CONFINED GEOMETRY

The catalytic reaction at the C sphere is responsible for a propulsion force along the dimer bond, which, for our choice of interaction parameters, results in a mean motor

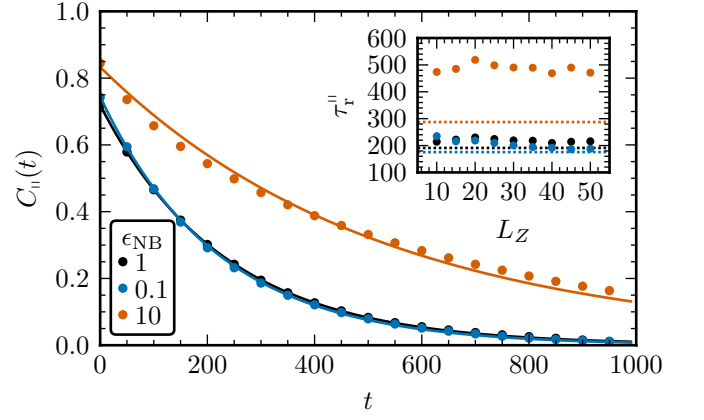


FIG. 6. Parallel orientational correlation function of a confined inactive dimer, and confined puller and pusher motors, for $L_Z = 20$ and $\epsilon_{wS} = 2$. The solid lines show fits to an exponential decay. The inset shows the fitted relaxation times τ_r as a function of L_Z . The dotted lines indicate τ_r for the respective bulk case.

velocity, $\langle V_z \rangle \neq 0$. The propulsion velocity of a puller motor is shown in Fig. 5 as a function of the distance from the wall for various wall separations, L_Z . Close to the wall dimer propulsion is suppressed leading to smaller mean velocities of $\langle V_z \rangle \approx 0.023$. Far from the wall the velocity converges to a limit value $\langle V_z \rangle \approx 0.029$, which corresponds to the propulsion velocity of an unconfined puller motor. A dimer confined in a narrower slab with $L_Z \leq 20$ has a slightly smaller velocity close to the wall than a dimer confined in a wider slab, but overall the velocity profile is roughly independent of L_Z .

The dimer is subject to strong thermal fluctuations from the solvent that affect its translational and rotational motion. In particular, rotational Brownian motion will reorient the dimer motor so that its ballistic motion will only be manifested for times less than the average reorientation time. (In fact, for these Ångström-size dimer motors, the ballistic regime is dominated by thermal inertial effects.³²) For times longer than this, the behavior will be diffusive but with an enhanced diffusion coefficient. As discussed earlier, these reorientation effects are especially strong for Ångström-size dimers and the crossover from ballistic to diffusive motion occurs on the time scale of picoseconds. For a dimer motor confined by two parallel walls, rotational motion is no longer isotropic and it is interesting to examine how confinement influences this property.

If, as earlier, we denote by $\hat{\mathbf{z}}$ the unit vector along the dimer bond, we may resolve this quantity into its components perpendicular and parallel to the wall, $\hat{\mathbf{z}}_\perp$ and $\hat{\mathbf{z}}_\parallel$, respectively. Here we focus on the parallel component since the corresponding correlation function may be compared directly with that of an unconfined dimer. The parallel orientational correlation function, $C_{||}(t) = \langle \hat{\mathbf{z}}_\parallel(t) \cdot \hat{\mathbf{z}}_\parallel \rangle$, is plotted in Fig. 6 versus time for an inactive dimer, and

puller and pusher motors. The parallel orientational correlation follows an exponential decay, $C_{||}(t) \propto e^{-t/\tau_r^||}$, and the fitted relaxation times $\tau_r^||$ are shown in the inset of Fig. 6 as a function of the wall separation L_Z . For the inactive dimer and the puller motor, the confined and unconfined dimers exhibit roughly the same reorientation time. For the pusher motor, however, the relaxation times of the confined dimer are almost twice as large as for the unconfined dimer. The confinement between the two walls has a negligible effect on the parallel orientational correlation in the case of the inactive dimer and the puller motor, but a strong effect in the case of the pusher motor. We see this effect for both values of ϵ_{wS} .

As discussed above, one of the major, easily obtainable signatures of propulsion for very small motors is the existence of enhanced diffusion. Confinement will influence this transport property. We have shown earlier³² that the MSD of an unconfined Ångström-scale sphere-dimer motor exhibits an enhanced diffusive regime and is approximated well by the equation (d is now the number of dimensions)

$$\Delta L^2(t) = 2dD_m t - 2\langle V_z \rangle^2 \tau_r^2 \left(1 - e^{-t/\tau_r}\right) - 2d \frac{k_B T}{M_m} \tau_v^2 \left(1 - e^{-t/\tau_v}\right). \quad (5)$$

Here τ_v is the decay time of the velocity fluctuations as determined from the diffusion coefficient of an inactive dimer, $D_0 = (k_B T/M_m) \tau_v$. The MSD reduces to $\Delta L^2(t) \approx (dk_B T/M_m + \langle V_z \rangle^2) t^2$ in the ballistic regime, $t \ll \tau_v$, and to $\Delta L^2(t) \approx 2d(D_0 + \frac{1}{d}\langle V_z \rangle^2 \tau_r) t = 2dD_m t$ in the diffusive regime, $t \gg \tau_r$.³²

The MSDs of a confined inactive dimer, and confined puller and pusher motors are shown in Fig. 7. To account for the confined geometry, the MSDs are separated into components perpendicular and parallel to the walls, $\Delta L_{\perp}^2(t) = \langle (R_{\perp}(t) - R_{\perp})^2 \rangle$ and $\frac{1}{2}\Delta L_{||}^2(t) = \frac{1}{2}\langle |\mathbf{R}_{||}(t) - \mathbf{R}_{||}|^2 \rangle$, where $\mathbf{R}(t)$ is the center of mass of the dimer. For the inactive dimer and the puller motor, the parallel components show negligible dependence on L_Z and overlap with the one-dimensional MSD of the respective bulk case. For the pusher motor, the parallel components also show negligible dependence on L_Z but deviate significantly from the MSD of the bulk case. In contrast to the parallel components, the perpendicular components show L_Z -dependent behavior. For the inactive dimer, the perpendicular MSDs reach a diffusive regime for intermediate times for all but the smallest $L_Z = 10$, and the diffusion coefficient decreases with decreasing L_Z . For the puller motor, the perpendicular MSDs show the same qualitative behavior as the bulk MSD in the intermediate time regime; in the long-time limit, however, where the bulk MSD reaches the enhanced diffusive regime, the confined MSDs instead converge to L_Z -dependent limits, which are in good agreement with the theoretical limit $\frac{1}{6}\Delta L_Z^2$ of confined diffusion for a one-dimensional random walk.⁴⁷ For the pusher motor, the perpendicular MSDs show superdiffusive behavior in the

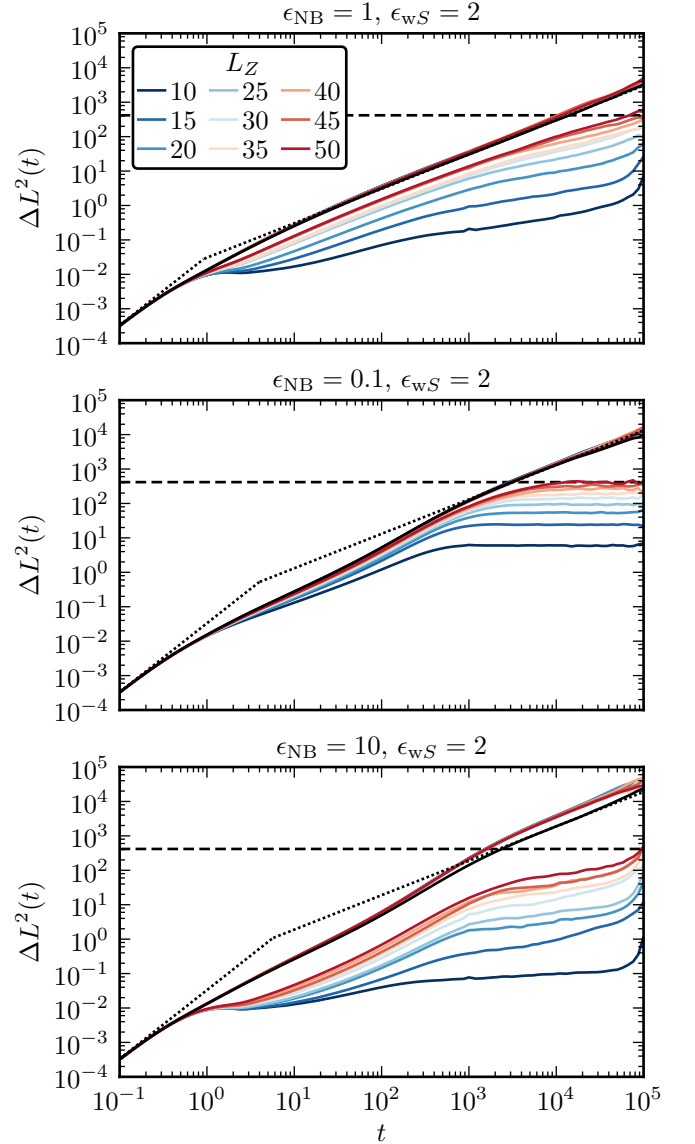


FIG. 7. One-dimensional mean square displacements parallel and perpendicular to walls depending on wall separation L_Z for an inactive dimer (top), and puller (middle) and pusher motors (bottom). In each panel, the ensemble of overlapping curves at the top corresponds to the parallel MSDs, and the diverging curves below correspond to the perpendicular MSDs. The solid black line corresponds to the one-dimensional MSD for an unconfined dimer. The dotted lines show the ballistic and diffusive regimes of the one-dimensional MSD for an unconfined dimer. The dashed, horizontal line indicates the theoretical limit of confined diffusion for $L_Z = 50$.

intermediate time regime; compared to the puller motor, however, the superdiffusive regime is strongly suppressed, and in the long-time limit, the MSDs become subdiffusive, to the point of a plateau for the smallest $L_Z = 10$ that is two orders of magnitude below $\frac{1}{6}\Delta L_Z^2$. The differences in the L_Z -dependence of the intermediate regimes of the perpendicular MSDs for the three cases follow from

L_Z	ϵ_{NB}	d	$\langle V_z \rangle$	τ_r^{\parallel}	D_m^{\parallel}	$\Delta D_{m,th}^{\parallel}$
10	1			214	0.019	
10	0.1	2	0.022	235	0.075	+1%
10	10	2	-0.022	474	0.192	-31%
20	1			230	0.017	
20	0.1	3	0.024	219	0.069	-12%
20	10	2	-0.021	519	0.199	-34%
30	1			219	0.018	
30	0.1	3	0.026	201	0.066	-5%
30	10	2	-0.021	490	0.180	-28%
40	1			209	0.017	
40	0.1	3	0.027	192	0.074	-14%
40	10	2	-0.022	469	0.184	-31%
50	1			215	0.018	
50	0.1	3	0.027	188	0.070	-8%
50	10	2	-0.022	471	0.175	-26%
∞	1			191	0.015	
∞	0.1	3	0.029	176	0.066	-1%
∞	10	3	-0.025	287	0.095	-23%

TABLE I. Dynamical properties for an inactive dimer, and puller and pusher motors, for various wall separations L_Z and $\epsilon_{wS} = 2$, and the bulk case: Mean propulsion velocity, $\langle V_z \rangle$, relaxation time of the parallel orientational correlation, τ_r^{\parallel} , diffusion constant of the parallel mean-square displacement, D_m^{\parallel} , and deviation of the theoretical estimate for the diffusion constant, $D_{m,th}^{\parallel} = D_0 + \frac{1}{d} \langle V_z \rangle^2 \tau_r^{\parallel}$, where d is the effective number of dimensions of the system that minimizes $\Delta D_{m,th}^{\parallel}$.

the different structural ordering of the dimer. As noted before, the puller motor frequently makes transitions between the walls for $\epsilon_{wS} = 2$, which results in long periods away from the walls with superdiffusive motion, and short periods close to the walls with suppressed motion perpendicular to the walls. The inactive dimer and the pusher motor, on the other hand, are trapped for very long periods (as long as our simulation times) after their first contact with a wall; their perpendicular MSDs reflect the averaging over the initial period of diffusive or superdiffusive motion, respectively, and the subsequent period of suppressed motion perpendicular to the walls. The time until first contact grows with L_Z and is larger for the inactive dimer than the motor dimers due to the absence versus presence of propulsion, which explains the more strongly suppressed perpendicular MSDs for the pusher motor compared to the inactive dimer.

The diffusion constants extracted from the parallel MSDs of confined dimers and the MSD of unconfined dimers are listed in Table I; along with the motor velocities, the reorientation times parallel to the walls, and theoretical estimates for the diffusion constant from these quantities. For the inactive dimer and the puller motor, the diffusion constants D_m^{\parallel} of the confined and unconfined dimers are approximately equal; for the pusher motor, the diffusion constant of the confined dimer is twice that of the unconfined dimer. The effective number of dimensions d in the theoretical estimate for the diffusion constant, $D_m^{\parallel} = D_0 + \frac{1}{d} \langle V_z \rangle^2 \tau_r^{\parallel}$, is chosen as 2 for the

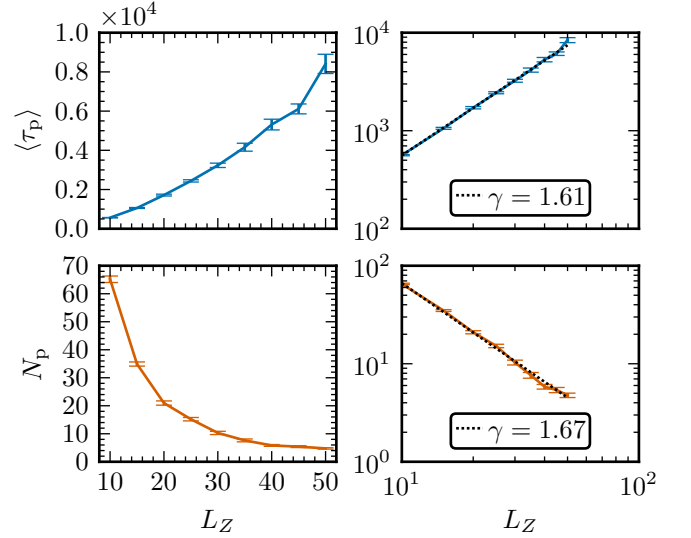


FIG. 8. Mean first-passage time (top) and number of passages (bottom) of a puller motor between opposite wall regions as a function of L_Z , for $\epsilon_{wS} = 2$. The center of mass of the dimer is considered to be in a wall region when the distance from the wall $\zeta < 2.5$. The right panels show fits to power laws, $\langle \tau_p \rangle \propto L_Z^\gamma$ and $N_p \propto L_Z^{-\gamma}$.

pusher motor, which is trapped by a wall most of the time, and 2 or 3, depending on L_Z , for the puller motor, which for small L_Z spends most of the time in the wall regions. For the puller motor, the theoretical values of D_m^{\parallel} are in good agreement with the measured values. For the pusher motor, the theoretical values consistently underestimate the measured values, which, however, is also the case for the unconfined pusher motor; hence, this deviation is not specific to the confinement. Since the reorientation times for the pusher motor deviate substantially from those of the inactive dimer, this indicates that reorientation also has an active component. The simple estimate for diffusion enhancement assumes simple inactive reorientation and this is likely the origin of the quantitative failure of the simple theoretical estimate for the pusher motor. Nevertheless, these considerations suggest that the increased τ_r^{\parallel} of the confined pusher motor is responsible for the increased D_m^{\parallel} compared to the bulk case.

For the puller motor that makes frequent transitions between the walls, the mean first-passage time and the number of passages are plotted as a function of L_Z in Fig. 8. The first-passage time and the number of passages are found to follow power laws, $\langle \tau_p \rangle \propto L_Z^\gamma$ and $N_p \propto L_Z^{-\gamma}$, respectively, with exponent $\gamma \approx 1.6$, which indicates superdiffusive transitions between the walls.⁴⁸

V. CONCLUSION

Molecular motors effect active transport in the cell and carry out a variety of other cellular functions. It is certainly interesting to imagine that, in the future, synthetic molecular-scale motors and machines could also be used for biological functions at the cellular level. The fact that the dynamical properties of small catalysts and single enzyme molecules are modified by chemical activity supports such a notion.^{27–29} While the potential applications of micron-scale motors are being actively explored and many of their properties can be modeled through continuum theories, the dynamics of Ångström-size synthetic motors involve some additional considerations that can only be captured through full molecular dynamics simulations. They are dominated by fluctuations, molecular reorientation often occurs on picosecond time scales limiting the regime where ballistic motion dominates, solvent sizes are often comparable to those of the motor, so structural effects come into play and solvent depletion forces are very strong. These features, combined with the fact that the utility of a continuum description of the solvent velocity flow fields must be confirmed, make these active objects challenging to study.

On the Ångström scale, specific characteristics of the molecular nature of the motor and its environment become important. This implies that studies of real systems on these microscopic scales will have to account for these molecular details. The model system studied in this paper provides insight into some of the qualitative characteristics that such systems may exhibit. In particular, the results show how the distinctive features of Ångström-scale motors, in combination with confinement, change motor spatial structure and dynamics. We have seen that self-propulsion is able to counteract solvent depletion forces in some circumstances so that the structural ordering of inactive dimers between the walls is very different from that of active dimer motors. The strong anisotropy and spatial dependence of dynamical properties including motor velocity, orientation, and diffusion have their origin in the confining geometry. Such information should prove useful for applications involving very small motors in cellular or microfluidic environments.

ACKNOWLEDGMENTS

This work was supported in part by a grant from the Natural Sciences and Engineering Research Council of Canada and Compute Canada.

- ¹J. Wang, *Nanomachines: Fundamentals and Applications* (Wiley-VCH, Weinheim, 2013).
- ²R. A. L. Jones, *Soft Machines: Nanotechnology and Life* (Oxford University Press, Oxford, 2004).
- ³G. A. Ozin, I. Manners, S. Fournier-Bidoz, and A. Arsenault, *Adv. Mater.* **17**, 3011 (2005).
- ⁴Y. Hong, D. Velegol, N. Chaturvedi, and A. Sen, *Phys. Chem. Chem. Phys.* **12**, 1423 (2010).

- ⁵R. Kapral, *J. Chem. Phys.* **138**, 020901 (2013).
- ⁶M. García, J. Orozco, M. Guix, W. Gao, S. Sattayasamitsathit, A. Escarpa, A. Merkoçi, and J. Wang, *Nanoscale* **5**, 1325 (2013).
- ⁷S. S. D. Patra, W. Duan, H. Zhang, R. Pavlick, and A. Sen, *Nanoscale* **5**, 1273 (2013).
- ⁸W. Gao and J. Wang, *Nanoscale* **6**, 10486 (2014).
- ⁹J. Palacci, C. Cottin-Bizonne, C. Ybert, and L. Bocquet, *Phys. Rev. Lett.* **105**, 088304 (2010).
- ¹⁰I. Theurkauff, C. Cottin-Bizonne, J. Palacci, C. Ybert, and L. Bocquet, *Phys. Rev. Lett.* **108**, 268303 (2012).
- ¹¹L. F. Valadares, Y.-G. Tao, N. S. Zacharia, V. Kitaev, F. Galembeck, R. Kapral, and G. A. Ozin, *Small* **6**, 565 (2010).
- ¹²S. Sengupta, D. Patra, I. Ortiz-Rivera, A. Agrawal, S. Shklyaev, K. K. Dey, U. Córdova-Figueroa, T. E. Mallouk, and A. Sen, *Nature Chem.* **6**, 415 (2014).
- ¹³M. N. Popescu, S. Dietrich, and G. Oshanin, *J. Chem. Phys.* **130**, 194702 (2009).
- ¹⁴G. Volpe, I. Buttinoni, D. Vogt, H.-J. Kümmerer, and C. Bechinger, *Soft Matter* **7**, 8810 (2011).
- ¹⁵W. E. Uspal, M. N. Popescu, S. Dietrich, and M. Tasinkevych, *Soft Matter* **11**, 434 (2015).
- ¹⁶D. G. Crowdy, *J. Fluid Mech.* **735**, 473 (2013).
- ¹⁷P. Ghosh, V. Misko, F. Marchesoni, and F. Nori, *Phys. Rev. Lett.* **110**, 268301 (2013).
- ¹⁸P. K. Ghosh, *J. Chem. Phys.* **141**, 061102 (2014).
- ¹⁹J. Elgeti and G. Gompper, *EPL* **85**, 38002 (2009).
- ²⁰J. Elgeti and G. Gompper, *EPL* **101**, 48003 (2013).
- ²¹H. H. Wensink and H. Löwen, *Phys. Rev. E* **78**, 031409 (2008).
- ²²E. Lauga and T. R. Powers, *Rep. Prog. Phys.* **72**, 096601 (2009).
- ²³S. E. Spagnolie and E. Lauga, *J. Fluid Mech.* **700**, 105 (2012).
- ²⁴J. P. Hernandez-Ortiz, C. G. Stoltz, and M. D. Graham, *Phys. Rev. Lett.* **95**, 204501 (2005).
- ²⁵J. P. Hernandez-Ortiz, P. T. Underhill, and M. D. Graham, *J. Phys.: Condens. Matter* **21**, 204107 (2009).
- ²⁶A. Zöttl and H. Stark, *Phys. Rev. Lett.* **112**, 118101 (2014).
- ²⁷R. A. Pavlick, K. K. Dey, A. Sirjoosingh, A. Benesi, and A. Sen, *Nanoscale* **5**, 1301 (2013).
- ²⁸H. S. Muddana, S. Sengupta, T. E. Mallouk, A. Sen, and P. J. Butler, *J. Am. Chem. Soc.* **132**, 2110 (2010).
- ²⁹S. Sengupta, K. K. Dey, H. S. Muddana, T. Tabouillot, M. E. Ibele, P. J. Butler, and A. Sen, *J. Am. Chem. Soc.* **135**, 1406 (2013).
- ³⁰T.-C. Lee, M. Alarcón-Correa, C. Miksch, K. Hahn, J. G. Gibbs, and P. Fischer, *Nano Lett.* **14**, 2407 (2014).
- ³¹S. Gáspár, *Nanoscale* **6**, 7757 (2014).
- ³²P. H. Colberg and R. Kapral, *EPL* **106**, 30004 (2014).
- ³³J. L. Anderson and D. C. Prieve, *Sep. Purif. Rev.* **13**, 67 (1984).
- ³⁴J. L. Anderson, *Ann. Rev. Fluid Mech.* **21**, 61 (1989).
- ³⁵R. Golestanian, T. B. Liverpool, and A. Ajdari, *Phys. Rev. Lett.* **94**, 220801 (2005).
- ³⁶G. Rückner and R. Kapral, *Phys. Rev. Lett.* **98**, 150603 (2007).
- ³⁷Y.-G. Tao and R. Kapral, *J. Chem. Phys.* **128**, 164518 (2008).
- ³⁸P. H. Colberg, S. Y. Reigh, B. Robertson, and R. Kapral, *Acc. Chem. Res.* **47**, 3504 (2014).
- ³⁹M. Yang, A. Wysockia, and M. Ripoll, *Soft Matter* **10**, 6208 (2014).
- ⁴⁰M. N. Popescu, M. Tasinkevych, and S. Dietrich, *EPL* **95**, 28004 (2011).
- ⁴¹S. Y. Reigh and R. Kapral, *Soft Matter* **11**, 3149 (2015).
- ⁴²The simulations were run on GPUs using a massively parallel code written in OpenCL C and Lua, which is distributed under a free software license at <http://colberg.org/angstrom-dimer>.
- ⁴³In applications to experimental systems the specific properties of the intermolecular potentials should be taken into account.
- ⁴⁴A. Rahman, *Phys. Rev.* **136**, A405 (1964).
- ⁴⁵H. N. Lekkerkerker and R. Tuinier, *Colloids and the Depletion Interaction* (Springer Netherlands, 2011).
- ⁴⁶Ensemble averages were carried out over 30 realisations of each 10^8 integration steps for a given system L_Z , ϵ_{NB} , and ϵ_{WS} .
- ⁴⁷T. Bickel, *Physica A* **377**, 24 (2007).

⁴⁸A comparable scaling behavior has been derived for an unrelated system with superdiffusive transport, where the first-passage time is found to follow a power law with exponent $\frac{4}{3}$.⁴⁹

⁴⁹J.-P. Bouchaud, A. Georges, J. Koplik, A. Provata, and S. Redner, *Phys. Rev. Lett.* **64**, 2503 (1990).